IRWIN AND JOAN JACOBS
CENTER FOR COMMUNICATION AND INFORMATION TECHNOLOGIES

Fast 3D radiative transfer tomography

Aviad Levis, Yoav Y. Schechner, Amit Aides, Anthony B. Davis

CCIT Report #876
December 2014

Electronics
Computers
Communications

DEPARTMENT OF ELECTRICAL ENGINEERING
TECHNION - ISRAEL INSTITUTE OF TECHNOLOGY, HAIFA 32000, ISRAEL

CCIT Report #876 December 2014

Fast 3D radiative transfer tomography

Aviad Levis, Yoav Y. Schechner, Amit Aides, Anthony B. Davis

Abstract

This paper introduces a method to preform optical tomography in 3D, using radiative transfer as the forward model. We use an iterative approach to solve the optimization problem in a scalable manner. Finally we show an application in remote sensing of the atmosphere.

1 Introduction

Optical tomography is an imaging technique that uses optical measurements on the boundary of a domain, to find the spatial distribution of parameters within. It finds applications in bio-medical imaging and remote sensing of the earth atmosphere [1–4]. For a list of applications we refer the reader to [5, 6] and the references therein. Solving the inverse problem using the radiative transfer equation (RTE) as a forward model can be difficult and computationally demanding. For some applications it is possible to use an approximate model. In dense media (mean free path small compared the distance of propagation), with scattering dominant over absorption, it is possible to use a diffusion approximation of the RTE. This results in the inverse problem of *Diffuse Optical Tomography* (DOT) [7–9]. When the mean free path is large compared to the propagation distance, the measured energy is dominated by direct and single scattered intensities. The resulting inverse problem is single scattering tomography [6, 10, 11]. Other approximations and their derivations can be found in [12]. We wish to solve the inverse problem using the RTE, with neither single scattering, nor diffusion approximations. However, a numerical solution of the RTE in 3D is time consuming. Therefore, to make the inverse problem tractable, we derive an iterative optimization framework.

2 Theoretical background

2.1 Radiative transfer

Our forward model is the time-independent radiative transfer. This model is used in passive imaging, such as atmospheric tomography, or when source gating is sufficiently slow. The RTE governs propagation of light through a medium. Consider a domain Ω having boundary $\partial\Omega$ whose outward facing normal is $\boldsymbol{\vartheta}$ (Fig. 1a). The domain is indicated by position $\boldsymbol{x} \in \mathbb{R}^3$ and direction $\boldsymbol{\omega} \in \mathbb{S}^2$ (unit sphere). The radiation (light)

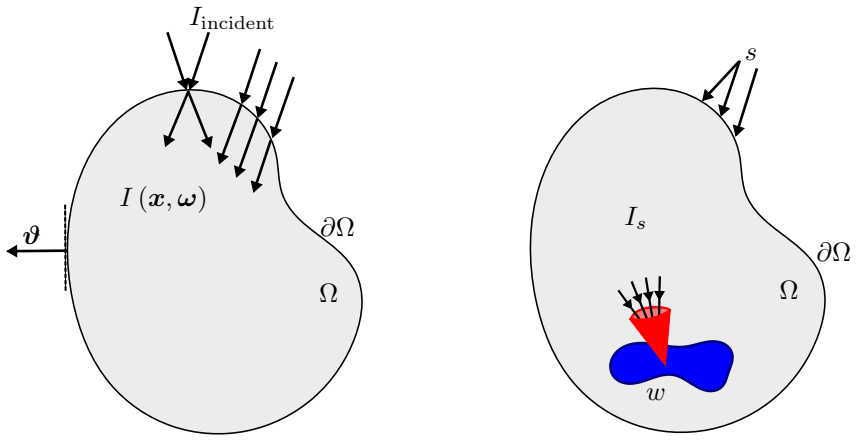

Figure 1: (a) Domain and boundary conditions; (b) Aperture function. Blue marks the spatial support and red marks the angular support

field is $I^{\lambda}(\boldsymbol{x},\boldsymbol{\omega})$. The superscript λ indicates wave-length dependency and will be omitted from here on, for simplicity. A boundary condition (Fig. 1a) is

$$I(\boldsymbol{x},\boldsymbol{\omega}) = I_{\text{incident}}(\boldsymbol{x},\boldsymbol{\omega}) \qquad \text{if} \quad \boldsymbol{\omega}\cdot\boldsymbol{\vartheta} < 0, \quad \boldsymbol{x}\in\partial\Omega, \tag{1}$$

where $\boldsymbol{\omega}\cdot\boldsymbol{\vartheta} < 0$ defines incoming radiation. In the absence of emission within the domain, the propagation of light is formulated in terms of the following conservation law [13, 14]:

$$\boldsymbol{\omega}\cdot\nabla I(\boldsymbol{x},\boldsymbol{\omega}) = \beta(\boldsymbol{x})\left[J(\boldsymbol{x},\boldsymbol{\omega}) - I(\boldsymbol{x},\boldsymbol{\omega})\right] \quad x\in\Omega, \tag{2}$$

where $\boldsymbol{\beta}$ is the extinction coefficient. Here $J(\boldsymbol{x},\boldsymbol{\omega})$ is called the *source function* or *in-scattering* term, since it accounts of an increase of radiation due to in-scattering. It is

$$J(\boldsymbol{x},\boldsymbol{\omega}) = \frac{\varpi}{4\pi}\int_{\mathbb{S}^2} p(\boldsymbol{\omega}\cdot\boldsymbol{\omega}')\, I(\boldsymbol{x},\boldsymbol{\omega}')\, d\boldsymbol{\omega}', \tag{3}$$

where ϖ is the single scattering albedo and $p(\boldsymbol{\omega}\cdot\boldsymbol{\omega}')$ is the phase function. The phase function describes the probability of a photon traveling in direction $\boldsymbol{\omega}'$ to scatter[1] to direction $\boldsymbol{\omega}'$. The phase function satisfies a normalization condition

$$\frac{1}{4\pi}\int_{\mathbb{S}^2} p(\boldsymbol{\omega}\cdot\boldsymbol{\omega}')\, d\boldsymbol{\omega}' = 1. \tag{4}$$

[1]In principle the phase function depends on both incoming and outgoing directions $(\boldsymbol{\omega},\boldsymbol{\omega}')$. However, dependency is often assumed to be solely on the scattering angle, equivalent to $\boldsymbol{\omega}\cdot\boldsymbol{\omega}'$.

Operator	Symbol	Domain	Range
Radiance forward mapping	$\boldsymbol{\mathcal{I}}$	Θ - Extinction fields	$\mathcal{Z}$ - Radiance fields
Measurement	$\boldsymbol{\mathcal{M}}$	$\mathcal{Z}$ - Radiance fields	$\mathcal{Y}$ - Measurements
Forward operator	$\boldsymbol{\mathcal{F}}$	Θ - Extinction fields	$\mathcal{Y}$ - Measurements
Scatter forward mapping	$\boldsymbol{\mathcal{J}}$	Θ - Extinction fields	$\mathcal{V}$ - Scatter fields
Transformation operator	$\boldsymbol{\mathcal{T}}$	$\mathcal{V}$ - Scatter fields	$\mathcal{Z}$ - Radiance fields

Table 1: Operator notation summary

Eq. (2) and it's corresponding boundary condition (1), define a radiative transfer forward model. Integrating Eq. (2) along a specific direction $\boldsymbol{\omega}$ results in the integral form of the RTE [14]

$$I(\boldsymbol{x},\boldsymbol{\omega}) = I_0 \exp\left[-\int_{\boldsymbol{x}}^{\boldsymbol{x}_0} \beta\left(\boldsymbol{r}\right) d\boldsymbol{r}\right] + \\ + \int_{\boldsymbol{x}}^{\boldsymbol{x}_0} J(\boldsymbol{x}',\boldsymbol{\omega})\beta\left(\boldsymbol{x}'\right) \exp\left[-\int_{\boldsymbol{x}}^{\boldsymbol{x}'} \beta\left(\boldsymbol{r}\right) d\boldsymbol{r}\right] d\boldsymbol{x}', \tag{5}$$

Where $\boldsymbol{x}_0$ is a point on the boundary and I_0 holds the boundary condition (1).

2.2 Operator Notation

We follow the definitions of [6] to formulate the forward model using operator notations (Table 1 summarizes the notations). Denote by Θ the space of extinction fields over the domain Ω. Let $\beta\left(\boldsymbol{x}\right) \in \Theta$ be an extinction field over the domain Ω. Let $\mathcal{S}$ represent a set of radiation sources over $\partial\Omega$. For a given source $s \in \mathcal{S}$, denote $\mathcal{Z}_s$ as the set of all possible radiation fields that satisfy Eqs. (1,2) across all possible $\beta \in \Theta$. The set $\mathcal{Z}_s$ is infinite, since for each extinction field $\beta(\boldsymbol{x})$ there is a corresponding radiation field $I_s = \boldsymbol{\mathcal{I}}_s\left(\beta\right)$. More generally the *radiance forward mapping*, $\boldsymbol{\mathcal{I}} : \Theta \to \mathcal{Z}$, is a mapping from the optical parameter domain, to the radiance field range $\mathcal{Z} = \bigcup_s \mathcal{Z}_s$. Measurements are an operator $\boldsymbol{\mathcal{M}} : \mathcal{Z} \to \mathcal{Y}$, mapping the continuous function space to a vector space $\mathcal{Y}$. Consequently the forward operator $\boldsymbol{\mathcal{F}}$ is defined as

$$\boldsymbol{\mathcal{F}} = \boldsymbol{\mathcal{M}}\boldsymbol{\mathcal{I}} : \Theta \to \mathcal{Y}. \tag{6}$$

The measurement operator $\boldsymbol{\mathcal{M}}$ is defined by the detector's aperture function, $w \in \Omega \times \mathbb{S}^2$ (Fig. 1b). The aperture function defines the manner in which the detector collects radiance, over a spatial and angular support. A given aperture and source pair (w, s) yields an element

$$y_{w,s} = \boldsymbol{\mathcal{F}}_{w,s}\left(\beta\right) = \boldsymbol{\mathcal{M}}_w\boldsymbol{\mathcal{I}}_s\left(\beta\right) = \langle w, I_s\rangle_\Omega, \tag{7}$$

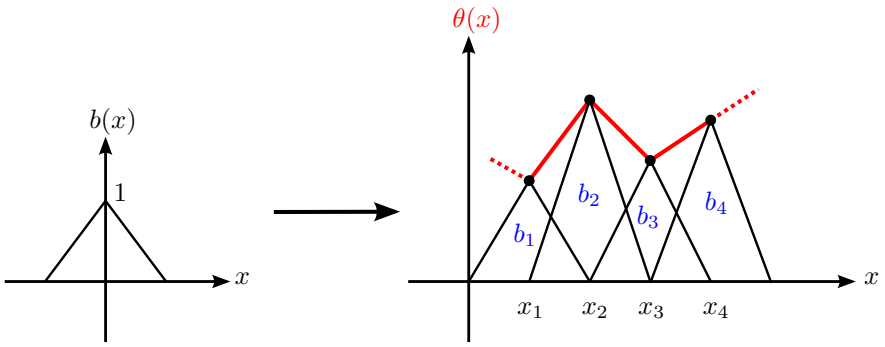

Figure 2: Illustration of a 1D linear interpolation kernel

for a specific extinction field β, where

$$\langle \cdot\,,\, \cdot \rangle_{\Omega} \equiv \int_{\Omega} \int_{\mathbb{S}^2} \cdot \cdot \, d\boldsymbol{\omega} d\boldsymbol{x}. \tag{8}$$

For an idealized single-pixel detector positioned at $\boldsymbol{x}^*$, collecting radiation flowing in direction $\boldsymbol{\omega}^*$,

$$y_{w,s} = \left\langle \delta\left(\boldsymbol{x} - \boldsymbol{x}^*\right) \delta\left(\boldsymbol{\omega} - \boldsymbol{\omega}^*\right)\,,\, I_s \right\rangle_{\Omega} = I_s\left(\boldsymbol{x}^*, \boldsymbol{\omega}^*\right). \tag{9}$$

We can define a matrix $\boldsymbol{Y}$ whose elements $y_{w,s}$ correspond to different source-detector configurations. A column of $\boldsymbol{Y}$ represents measurements by a single detector, for multiple sources. A row represents measurements by multiple detectors, for one particular light source. The vector $\boldsymbol{y}$ is the column stack of $\boldsymbol{Y}$.

2.3 Optical tomography

Using the operators defined in Sec. 2.2 we express the process of optical tomography. Tomographic reconstruction is an estimator of β that minimizes a defined cost

$$\hat{\beta} = \arg\min_{\beta} \left\{ \mathcal{E}\left[\boldsymbol{y}, \boldsymbol{\mathcal{F}}\left(\beta\right)\right] + \alpha \Psi\left(\beta\right) \right\}, \tag{10}$$

where $\mathcal{E}\left[\boldsymbol{y}, \boldsymbol{\mathcal{F}}\left(\beta\right)\right]$ is the *data fit* (fidelity) functional and $\Psi\left(\beta\right)$ is a *regularization* on the optical parameters. Here α is a tunable parameter, chosen in accordance with the noise level, to balance the two terms. Solving Eq. (10) for β

Except for a few special geometric configurations [6, 15], 3D tomographic recovery cannot be done analytically. Thus, the continuous function is often discretized (Fig. 2)

$$\beta\left(\boldsymbol{x}\right) = \sum_{k=1}^{N_{\text{grid}}} \beta_k b_k\left(\boldsymbol{x}\right), \tag{11}$$

where $\{\beta_k\}_{k=1}^{N_{\text{grid}}}$ are discrete parameters, $b_k(\boldsymbol{x})$ is an *interpolation kernel* and N_{grid} is the number of grid points used for discretization. We apply (11) to Eq. (10) to seek an estimator for $\boldsymbol{\beta} = \left(\beta_1, ..., \beta_{N_{\text{grid}}}\right)^T$, where $(\cdot)^T$ denotes transposition.

We focus here on gradient-based optimization methods. The forward operator $\boldsymbol{\mathcal{F}}$ is a non-linear function of the optical parameters. Thus, one approach [6, 16] estimates (10) by linearizing $\boldsymbol{\mathcal{F}}$. Suppose the solution is $\beta^{\delta} = \beta_0 + \delta\beta$, which is a perturbation of an initial guess β_0. It is possible to linearize $\boldsymbol{\mathcal{F}}$ and solve $\delta\beta$ using a linear set for equations. However, this approach requires an initial guess very close to the true solution. Another approach [17–20] iteratively estimates the gradient with respect to $\boldsymbol{\beta}$. However, this approach has high computational complexity, as it requires $\mathcal{O}(\mathcal{N}_{\text{grid}})$ simulations of the forward model per iteration (i.e for a single computation of the gradient). Forward model simulation is time consuming particularly in the presence of multiple scattering. Simulating the forward model per element of the gradient does not scale well as N_{grid} increases.

Our approach is also iterative, however each iteration is computationally simple, having run-time independent of N_{grid}. The approach does not directly optimize the nonlinear $\boldsymbol{\mathcal{F}}$. Instead, $\boldsymbol{\mathcal{I}}$ is decomposed into a product of two operators. Each is optimized in time. This concept is analogous to *EM-Like* optimization, which is used in DOT [21–23].

3 Optimization Approach

3.1 Forward map decomposition

In Sec. 2 the forward operator was defined in terms of the *radiance* field I. We now show that defining $\boldsymbol{\mathcal{F}}$ in terms of the *in-scatter* field J considerably speeds up the computation time. We decompose the radiance forward mapping into two operators, $\boldsymbol{\mathcal{I}} = \boldsymbol{\mathcal{T}}\boldsymbol{\mathcal{J}}$, which we now introduce. For a particular radiation source $s \in \mathcal{S}$, let $J_s = \boldsymbol{\mathcal{J}}_s(\beta)$ be the in-scatter field that satisfies Eq. (3), while I_s satisfies Eqs. (1,2). Define $\mathcal{V}_s$ as the set of possible in-scatter fields for a particular source. The *in-scatter forward mapping*, $\boldsymbol{\mathcal{J}} : \Theta \to \mathcal{V}$, is a mapping from the optical parameter domain to the in-scatter field range $\mathcal{V} = \bigcup_s \mathcal{V}_s$. We define the following transformation operator

$$\boldsymbol{\mathcal{T}} : \mathcal{V} \to \mathcal{Z}, \qquad I_s = \boldsymbol{\mathcal{T}}(\beta) J_s. \tag{12}$$

Eq. (3) defines a relation between a given light field I and a corresponding in-scatter field J. The transformation operator $\boldsymbol{\mathcal{T}}$, defined by Eq. (5), defines the *inverse* relation: for a given in-scatter field J, a corresponding light field I is attained. Consequently we define the forward operator in terms of the in-scatter forward mapping

$$\boldsymbol{\mathcal{F}} = \boldsymbol{\mathcal{M}}\boldsymbol{\mathcal{T}}(\beta)\,\boldsymbol{\mathcal{J}}(\beta) : \Theta \to \mathcal{Y}. \tag{13}$$

Define ℓ as a line of sight from $\boldsymbol{x}^*$ in direction $-\boldsymbol{\omega}^*$ (Fig. 3a). For a convex spa-

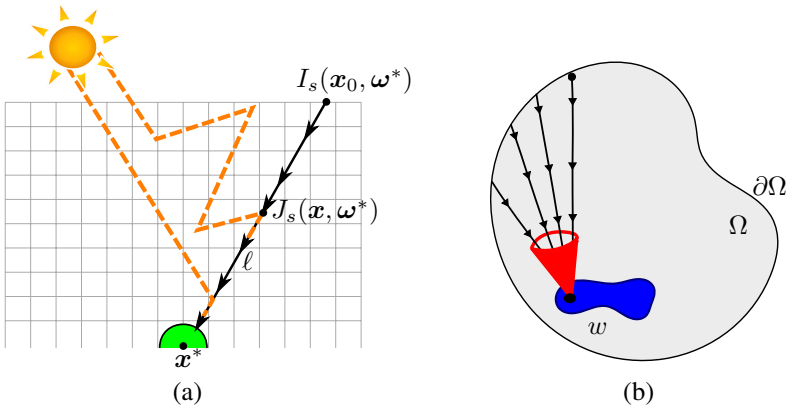

(a) (b)

Figure 3: (a) A line integral over the in-scatter field J_s. (b) Integration over the field f for an arbitrary aperture spatial and angular support w

tial domain, the intersection point between line of sight and the domain's boundary is unique and denoted by $\boldsymbol{x}_0 = \partial\Omega \cap \ell$ (Fig. 3a). Operator $\boldsymbol{\mathcal{T}}$ is defined by Eq. (5). For source $s \in \mathcal{S}$, the response of an idealized single pixel with aperture $w = \delta(\boldsymbol{x} - \boldsymbol{x}^*)\,\delta(\boldsymbol{\omega} - \boldsymbol{\omega}^*)$ is

$$\begin{aligned} y_{w,s} &= \boldsymbol{\mathcal{M}}_w \boldsymbol{\mathcal{T}} J_s \\ &= I_s(\boldsymbol{x}_0, \boldsymbol{\omega}^*) \exp\left[-\int_{\boldsymbol{x}^*}^{\boldsymbol{x}_0} \beta(\boldsymbol{r})\, d\boldsymbol{r}\right] + \int_{\boldsymbol{x}^*}^{\boldsymbol{x}_0} J_s(\boldsymbol{x}, \boldsymbol{\omega}^*) \beta(\boldsymbol{x}) \exp\left[-\int_{\boldsymbol{x}^*}^{\boldsymbol{x}} \beta(\boldsymbol{r})\, d\boldsymbol{r}\right] d\boldsymbol{x} \end{aligned} \tag{14}$$

The operation

$$\int_{\boldsymbol{x}^*}^{\boldsymbol{x}_0} f(\boldsymbol{x}) d\boldsymbol{x} \tag{15}$$

is a line-integral over a *field* $f(\boldsymbol{x})$. Numerically this is preformed by *back-projecting* (BP) a ray through a medium. Eq. (14) is simply an accumulation of the scattered radiance along the line of sight weighted by its corresponding attenuation factor (Fig. 3a). Applying a general measurement operation is a manner of integrating over the aperture function of the detector (Fig. 3b).

3.2 Iterative surrogate function optimization

Optimizing Eq. (10) directly over β is computationally expensive. Finding the gradient direction in each iteration requires $\mathcal{O}(\mathcal{N}_{\text{grid}})$ numerical computations of the forward model. With our approach, however, we iteratively keep J_s constant and estimate $\boldsymbol{\beta}$ solely based on $\boldsymbol{\mathcal{T}}$. Instead of optimizing through a function that is difficult to compute

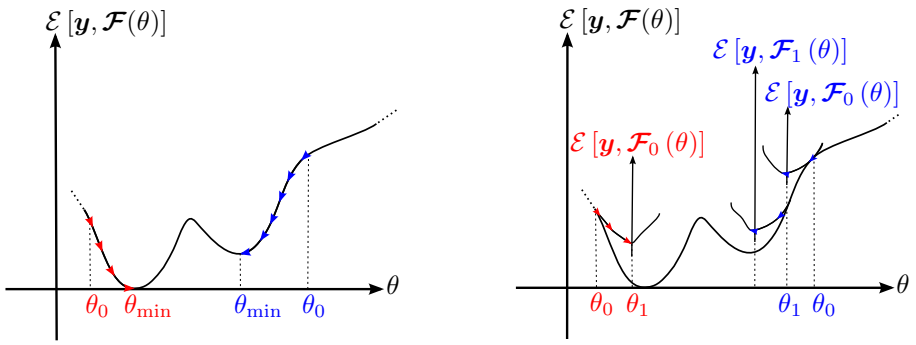

Figure 4: (a) Gradient decent optimization (b) Surrogate function iterative optimization; Both depend on the initial guess β_0

(Fig. 4b) we optimize $\boldsymbol{\beta}$ using a *surrogate function* [24], which is efficiently computed (Fig. 4a). We define the following iterative optimization process. Define β_n as an estimate of β in the "n" iteration. The first step, consists of computing the in-scatter field which corresponds to the current estimate β_n

$$J_n = \boldsymbol{\mathcal{J}}(\beta_n)$$

In the second step, keeping the in-scatter field constant, we solve the following optimization problem to find our next estimate of β

$$\begin{aligned}\beta_{n+1} &= \arg\min_{\beta} \left\{ [\boldsymbol{y} - \boldsymbol{\mathcal{M}}\boldsymbol{\mathcal{T}}(\beta) J_n]^T \boldsymbol{\Sigma}_{\text{meas}}^{-1} [\boldsymbol{y} - \boldsymbol{\mathcal{M}}\boldsymbol{\mathcal{T}}(\beta) J_n] + \alpha \Psi(\beta) \right\} \quad (16)\\ &= \arg\min_{\beta} \left\{ \mathcal{E}[\boldsymbol{y}, \boldsymbol{\mathcal{F}}_n(\beta)] + \alpha \Psi(\beta) \right\},\end{aligned}$$

Where

$$\boldsymbol{\mathcal{F}}_n(\beta) = \boldsymbol{\mathcal{M}}\boldsymbol{\mathcal{T}}(\beta) J_n, \quad (17)$$

is the n^{th} surrogate function, and $\boldsymbol{\Sigma}_{\text{meas}}^{-1}$ is the covariance matrix of our measurements.

Eq. (16) defines an iterative optimization process,

i. Start with an initial guess β_0.
ii. Based on the current estimate β_n, numerically find the in-scatter field $J_n = \boldsymbol{\mathcal{J}}(\beta_n)$.
iii. Optimize (16) to find the next estimate β_{n+1}.
iv. Repeat steps ii–iii until convergence.

3.3 Scalability

For a given measurement vector $\boldsymbol{y} \in \mathcal{Y}$, we solve the optimization of (16) with a gradient-based method. We use the discretization described in (11). Assuming uncorrelated measurements

$$\boldsymbol{\Sigma}_{\text{meas}} = \text{diag}(\boldsymbol{\sigma}_{\text{meas}}^2), \qquad \boldsymbol{\sigma}_{\text{meas}}^2 = \left(\sigma_1^2, ..., \sigma_{N_{\text{meas}}}^2\right)^T, \quad (18)$$

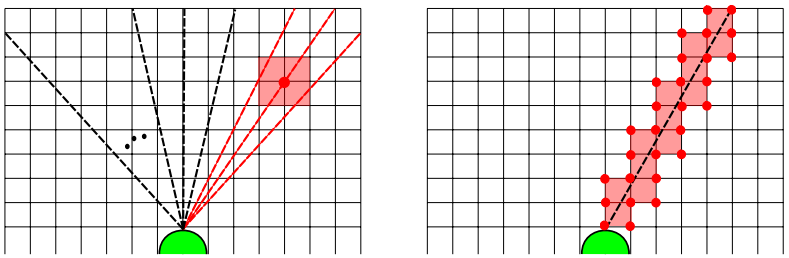

(a) (b)

Figure 5: (a) Each gradient element is computed by tracing all the rays. Only the red rays contribute to the computation of the red grid point gradient. (b) A single trace of each ray is performed. While tracing each ray we compute the gradient contribution to each relevant grid point

where $N_{\text{meas}} = N_w + N_s$ is the number of measurements, N_w is the number of detectors and N_s is the number of sources. The task is thus to recover the gridded extinction $\{\beta_k\}_{k=1}^{N_{\text{grid}}}$. For this purpose we find the k'th gradient element. Without loss of generality we formulate the problem in terms of a single source and many detectors.

$$\frac{\partial}{\partial \beta_k} \mathcal{E}\left[\boldsymbol{y}, \boldsymbol{\mathcal{F}}_n\left(\boldsymbol{\beta}\right)\right] = \sum_{w=1}^{N_{\text{meas}}} \frac{1}{\sigma_w^2} \left[\boldsymbol{\mathcal{F}}_n\left(\boldsymbol{\beta}\right) - y_w\right] \boldsymbol{\mathcal{M}}_w \left[\frac{\partial}{\partial \beta_k} \boldsymbol{\mathcal{T}}\left(\boldsymbol{\beta}\right)\right] J_n, \tag{19}$$

For an ideal single-pixel detector positioned at $\boldsymbol{x}^*$, collecting radiation flowing in direction $\boldsymbol{\omega}^*$ we get

$$\boldsymbol{\mathcal{M}}_w \left[\frac{\partial}{\partial \beta_k} \boldsymbol{\mathcal{T}}\left(\boldsymbol{\beta}\right)\right] J_n = A_{w,k} + B_{w,k} \tag{20}$$

where

$$A_{w,k} = \left[-\int_{\boldsymbol{x}^*}^{\boldsymbol{x}_0} b_k\left(\boldsymbol{r}\right) d\boldsymbol{r}\right] I(\boldsymbol{x}_0, \boldsymbol{\omega}^*) \exp\left[-\int_{\boldsymbol{x}^*}^{\boldsymbol{x}_0} \beta\left(\boldsymbol{r}\right) d\boldsymbol{r}\right] \tag{21}$$

and

$$B_{w,k} = \int_{\boldsymbol{x}^*}^{\boldsymbol{x}_0} J_n\left(\boldsymbol{x}, \boldsymbol{\omega}^*\right) \left[b_k(\boldsymbol{x}) - \beta(\boldsymbol{x}) \int_{\boldsymbol{x}^*}^{\boldsymbol{x}} b_k\left(\boldsymbol{r}\right) d\boldsymbol{r}\right] \exp\left[-\int_{\boldsymbol{x}^*}^{\boldsymbol{x}} \beta\left(\boldsymbol{r}\right) d\boldsymbol{r}\right] d\boldsymbol{x}. \tag{22}$$

Term A results from the boundary illumination and can be readily computed. Term B defines a line-integral over a field, computed using back-projection of rays from the detector through the medium. A straight-forward approach calculates each element of the gradient vector by summing all the back-projected rays from all the detectors (Alg. 2a). The complexity of this approach is $\mathcal{O}\left(\mathcal{N}_{\text{meas}} \times \mathcal{N}_{\text{grid}}\right)$ back-projecting operations. However, most of back-projected rays do not contribute to B since the interpolation kernel $b_k(\boldsymbol{x})$ typically has a small support region (Fig. 5a). Instead, for

1: **for** $k = 1 \rightarrow N_{\text{grid}}$ **do**
2: $\quad \text{Grad}_k = 0$
3: $\quad$ **for** $w = 1 \rightarrow N_{\text{meas}}$ **do**
4: $\quad\quad$ BP to compute $A_{w,k}$, $B_{w,k}$
5: $\quad\quad \text{Err} = \frac{1}{\sigma_w^2} \left[\boldsymbol{\mathcal{F}}_n \left(\boldsymbol{\beta} \right) - y_w \right]$
6: $\quad\quad \text{Grad}_k = \text{Grad}_k + \text{Err} \left(A_{w,k} + B_{w,k} \right)$
7: $\quad$ **end for**
8: **end for**

(a) Straight forward approach

1: $\text{Grad} = \mathbf{0}$
2: **for** $w = 1 \rightarrow N_{\text{meas}}$ **do**
3: $\quad \text{Err} = \frac{1}{\sigma_w^2} \left[\boldsymbol{\mathcal{F}}_n \left(\boldsymbol{\beta} \right) - y_w \right]$
4: $\quad$ **for** $k \in$ Support region **do**
5: $\quad\quad$ BP to compute $A_{w,k}$,$B_{w,k}$
6: $\quad\quad \text{Grad}_k = \text{Grad}_k + \text{Err} \left(A_{w,k} + B_{w,k} \right)$
7: $\quad$ **end for**
8: **end for**

(b) Scalable approach

Alg. 2: Comparison of the two approaches to compute the gradient of the surrogate function. $\text{Grad} = \left(\text{Grad}_1, ..., \text{Grad}_{N_{\text{grid}}} \right)$

each point along a ray we define a support region of grid points, according to the support region of the interpolation kernel (Fig. 5b). A specific ray will contribute to the computation of gradient elements associated with the grid points in the support region. In the case of linear interpolation kernel, a support region is composed of the eight corner grid points that make a grid cell. Since the support region is typically small, for each point along the ray we only need to look at a finite amount of neighboring grid points (Alg. 2b). The complexity of this approach is $\mathcal{O} \left(\mathcal{N}_{\text{meas}} \right)$ back-projecting operations. Hence, the computational complexity is independent of the number of grid points which makes this approach scalable.

4 Application to remote sensing

4.1 General setup

We use *large eddy simulation* (LES) [25, 26] to generate the microphysical quantities of a realistic cloud field (Fig .6). We use Mie scattering to transform the microphysical quantities (liquid water content, effective droplet radius) to optical quantities (extinction, phase function, single-scattering albedo). We add the extinction and phase function due to molecular scattering by air molecules (*Rayleigh* scattering). We seek to recover the extinction of the cloud droplets on a cartesian grid, where the air is taken to be a known parameter dependent only on the height. The boundary conditions for the domain are

- Sun radiation at the top of the atmosphere (TOA), at a zenith angle of $60 \deg$.
- Open boundary for the side faces.
- *Lambertian* reflectance at the surface (earth) with albedo of 0.05.

In order to find the in-scatter field J_n, we use the *Spherical Harmonics Discrete Ordinates Method* (SHDOM) [27, 28].

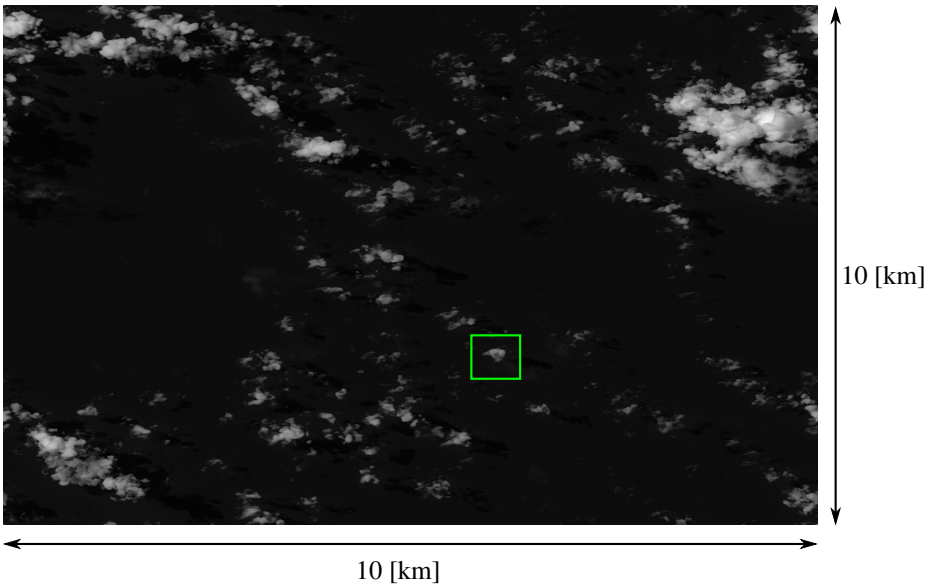

Figure 6: Cumulus cloud field generated by the LES. The image was generated with MYSTIC [29, 30] monte-carlo code. We focus on the retrieval of the cloud circled in green.

4.2 SHDOM

Running the forward model is a balance between speed and accuracy. Monte-Carlo methods, and can handle very complex optical phenomena. However, Monte-Carlo methods approximate radiometric quantities by random sampling the domain of possible light paths. This introduces stochastic noise at the output, which can be controlled by increasing the number of samples (photon paths). When many radiometric outputs of the same scene are sought, as in the case of many viewpoints, a model that solves the *RTE* directly has a much preferable run time [27]. A discrete ordinates representation models the flow of radiant energy in the domain easily and intuitively [28, 31, 32]. The SHDOM model uses a grid for the spatial dependency, and a linear interpolation kernel $b_k(\boldsymbol{x})$. *Spherical Harmonic* expansion [12, 33], computes angular integrals. SHDOM solves the forward model integro-differential equation for the source function. It can adaptively truncate negligible coefficients in the series expansion.

4.3 Simulation Results

We simulate an atmosphere of size $2\text{km} \times 0.72\text{km} \times 1.44\text{km}$. The unknown extinction is composed of $100 \times 136 \times 36$ grid points (129,600 unknowns). The measurements are taken to simulate the resolution of *airMSPI* (airborne multi-angle spectro-polarimeter imager) [34], which is an air-born instrument that samples the radiance at 20m resolution and at 9 view zenith angles: $(\pm 70.5, \pm 60, \pm 45.6, \pm 26.1, 0)$ (Fig. 7). We simulate

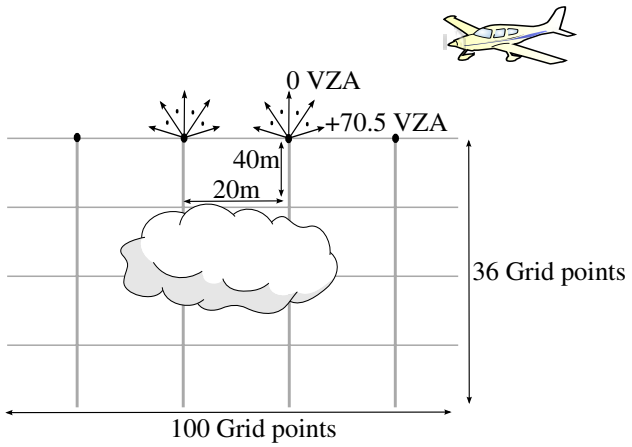

Figure 7: airMSPI measurements: 9 angles in the long track

the measurements using SHDOM for $672\mathrm{nm}$ wave-length, and add 3% gaussian noise to simulate the radiometric calibration noise, which is the dominant factor for this sensor. We initialize our algorithm with $\boldsymbol{\beta} = \mathbf{0}$ (an atmosphere containing only air molecules). The converged result is displayed in Fig. 8. Simulated images as viewed from the airMSPI instrument flying over the recovered cloud are shown in Fig. 9. We compare the total extinction recovered, which is relative to the total LWC, with the ground truth. We define a relative error measure

$$\text{Relative Error} = \frac{\boldsymbol{\beta}^{\text{groundtruth}} - \boldsymbol{\beta}^{\text{recovered}}}{\sum_k \beta_k^{\text{groundtruth}}}$$

The performance for the recovery is summarized in Table 3.

5 Discussion

We derive a novel iterative optimization method to perform radiative transfer tomography. The unknown β directly affects $\boldsymbol{\mathcal{T}}(\beta)$. From (5), this principle can only retrieve parameters that relate to the extinction. We cannot estimate the phase function using this formulation. Sec. 3.3 explains the computational advantage of this approach. We show an application to remote sensing of Earth's atmosphere (Sec. 4), however, this approach could potentially be applied to preform optical tomography of biological tissues. We use SHDOM as our forward mapping engine. Nevertheless, it is possible to use different radiative transfer engines, such as *Monte Carlo*. Further enhancement of scalability may be obtained by use of adjoint operators [35]. This is a subject intended for further research.

$\sum_k \beta_k^{\text{recovered}}$	9.8001e+04
$\sum_k \beta_k^{\text{groundtruth}}$	8.6062e+04
Sum of relative error	0.6055
Maximum relative error	8.0250e-04

Table 3: Recovery results

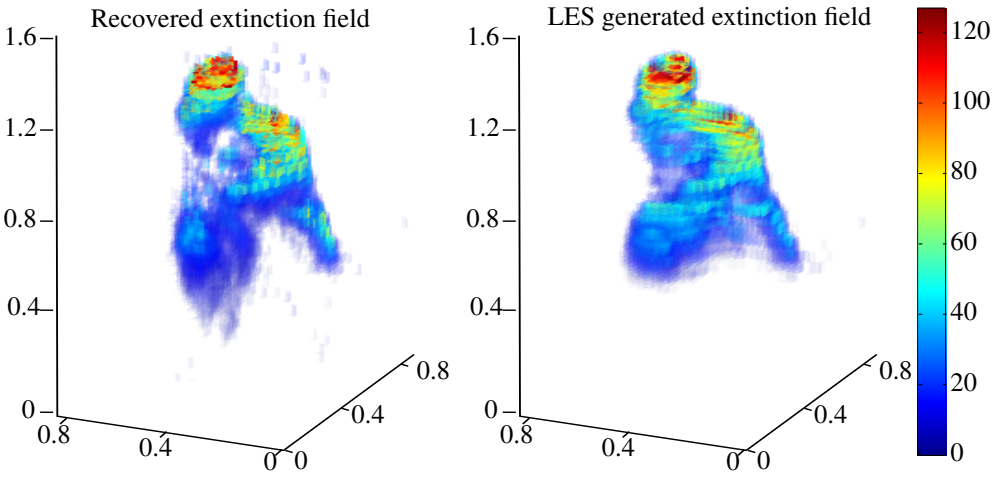

Figure 8: A volumetric comparison between the ground truth LES generated cloud and the recovered cloud

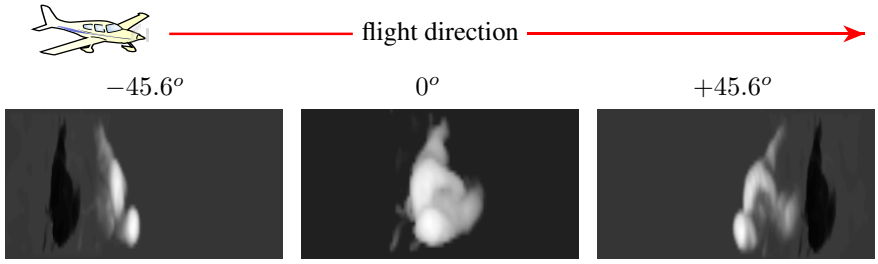

Figure 9: A simulated fly-over of the airMSPI using SHDOM to generate the radiance measurements at 9 viewing angels. The cloud extinction field is that of the recovered cloud.

References

[1] Nakajima, T., King, M.D.: Determination of the optical thickness and effective particle radius of clouds from reflected solar radiation measurements. part i: Theory. Journal of the atmospheric sciences **47**(15) (1990) 1878–1893

[2] Nakajima, T., King, M.D., Spinhirne, J.D., Radke, L.F.: Determination of the optical thickness and effective particle radius of clouds from reflected solar radiation measurements. part 2: Marine stratocumulus observations. (1991)

[3] Davis, A.B., Marshak, A.: Solar radiation transport in the cloudy atmosphere: a 3d perspective on observations and climate impacts. Reports on Progress in Physics **73**(2) (2010) 026801

[4] Platnick, S., King, M.D., Ackerman, S.A., Menzel, W.P., Baum, B.A., Riédi, J.C., Frey, R.A.: The modis cloud products: Algorithms and examples from terra. Geoscience and Remote Sensing, IEEE Transactions on **41**(2) (2003) 459–473

[5] Bal, G.: Inverse transport theory and applications. Inverse Problems **25**(5) (2009) 053001

[6] Arridge, S., Schotland, J.: Optical tomography: forward and inverse problems. arXiv preprint arXiv:0907.2586 (2009)

[7] Gibson, A., Hebden, J., Arridge, S.R.: Recent advances in diffuse optical imaging. Physics in medicine and biology **50**(4) (2005) R1

[8] Boas, D.A., Brooks, D.H., Miller, E.L., DiMarzio, C.A., Kilmer, M., Gaudette, R.J., Zhang, Q.: Imaging the body with diffuse optical tomography. Signal Processing Magazine, IEEE **18**(6) (2001) 57–75

[9] Ntziachristos, V., Yodh, A., Schnall, M., Chance, B.: Concurrent mri and diffuse optical tomography of breast after indocyanine green enhancement. Proceedings of the National Academy of Sciences **97**(6) (2000) 2767–2772

[10] Florescu, L., Schotland, J.C., Markel, V.A.: Single-scattering optical tomography. Physical Review E **79**(3) (2009) 036607

[11] Aides, A., Schechner, Y.Y., Holodovsky, V., Garay, M.J., Davis, A.B.: Multi sky-view 3d aerosol distribution recovery. Optics Express **21**(22) (2013) 25820–25833

[12] Han, W., Eichholz, J.A., Wang, G.: On a family of differential approximations of the radiative transfer equation. Journal of Mathematical Chemistry **50**(4) (2012) 689–702

[13] Varadan, V., Bringi, V., Varadan, V., Ishimaru, A.: Multiple scattering theory for waves in discrete random media and comparison with experiments. Radio science **18**(3) (1983) 321–327

[14] Chandrasekhar, S.: Radiative transfer. Courier Dover Publications (1960)

[15] Davis, A.B.: Cloud remote sensing with sideways looks: theory and first results using multispectral thermal imager data. In: AeroSense 2002, International Society for Optics and Photonics (2002) 397–405

[16] Xu, F., Davis, A.B., Sanghavi, S.V., Martonchik, J.V., Diner, D.J.: Linearization of markov chain formalism for vector radiative transfer in a plane-parallel atmosphere/surface system. Applied Optics **51**(16) (2012) 3491–3507

[17] Abdoulaev, G.S., Hielscher, A.H.: Three-dimensional optical tomography with the equation of radiative transfer. Journal of Electronic Imaging **12**(4) (2003) 594–601

[18] Gkioulekas, I., Zhao, S., Bala, K., Zickler, T., Levin, A.: Inverse volume rendering with material dictionaries. ACM Transactions on Graphics (TOG) **32**(6) (2013) 162

[19] Klose, A.D., Hielscher, A.H.: Iterative reconstruction scheme for optical tomography based on the equation of radiative transfer. Medical physics **26**(8) (1999) 1698–1707

[20] Park, H., Yoon, T.: Solution of the inverse radiation problem using a conjugate gradient method. International journal of heat and mass transfer **43**(10) (2000) 1767–1776

[21] Wang, C.: An em-like reconstruction method for diffuse optical tomography. International Journal for Numerical Methods in Biomedical Engineering **26**(9) (2010) 1099–1116

[22] Wang, C., Wang, Z.: Total variation regularization for the em-like image reconstruction algorithm of diffuse optical tomography. In: Biomedical Engineering and Informatics (BMEI), 2011 4th International Conference on. Volume 1., IEEE (2011) 545–549

[23] Cao, N., Nehorai, A., Jacobs, M.: Image reconstruction for diffuse optical tomography using sparsity regularization and expectation-maximization algorithm. Optics express **15**(21) (2007) 13695–13708

[24] Lange, K., Hunter, D.R., Yang, I.: Optimization transfer using surrogate objective functions. Journal of computational and graphical statistics **9**(1) (2000) 1–20

[25] Matheou, G., Chung, D.: Large-eddy simulation of stratified turbulence. part ii: Application of the stretched-vortex model to the atmospheric boundary layer. Journal of the Atmospheric Sciences (2014) (2014)

[26] Chung, D., Matheou, G.: Large-eddy simulation of stratified turbulence. part i: A vortex-based subgrid-scale model. Journal of the Atmospheric Sciences **71**(5) (2014) 1863–1879

[27] Evans, K.F.: The spherical harmonics discrete ordinate method for three-dimensional atmospheric radiative transfer. Journal of the Atmospheric Sciences **55**(3) (1998) 429–446

[28] Davis, A., Marshak, A.: 3D radiative transfer in cloudy atmospheres. Springer (2005)

[29] Buras, R., Mayer, B.: Efficient unbiased variance reduction techniques for monte carlo simulations of radiative transfer in cloudy atmospheres: The solution. Journal of quantitative spectroscopy and radiative transfer **112**(3) (2011) 434–447

[30] Mayer, B.: Radiative transfer in the cloudy atmosphere. In: EPJ Web of Conferences. Volume 1., EDP Sciences (2009) 75–99

[31] Truelove, J.: Discrete-ordinate solutions of the radiation transport equation. Journal of Heat Transfer (Transcations of the ASME (American Society of Mechanical Engineers), Series C);(United States) **109**(4) (1987)

[32] Sánchez, A., Smith, T., Krajewski, W.: A three-dimensional atmospheric radiative transfer model based on the discrete-ordinates method. Atmospheric research **33**(1) (1994) 283–308

[33] Kajiya, J.T., Von Herzen, B.P.: Ray tracing volume densities. In: ACM SIGGRAPH Computer Graphics. Volume 18., ACM (1984) 165–174

[34] Diner, D., Xu, F., Garay, M., Martonchik, J., Rheingans, B., Geier, S., Davis, A., Hancock, B., Jovanovic, V., Bull, M., et al.: The airborne multiangle spectropolarimetric imager (airmspi): a new tool for aerosol and cloud remote sensing. Atmospheric Measurement Techniques **6**(8) (2013) 2007–2025

[35] Martin, W., Cairns, B., Bal, G.: Adjoint methods for adjusting three-dimensional atmosphere and surface properties to fit multi-angle/multi-pixel polarimetric measurements. Journal of Quantitative Spectroscopy and Radiative Transfer **144** (2014) 68–85